Inflammatory dendritic cells migrate in and out of transplanted chronic mycobacterial granulomas in mice

Heidi A. Schreiber,[1,2] Jeffrey S. Harding,[1,2] Oliver Hunt,[1] Christopher J. Altamirano,[1,3] Paul D. Hulseberg,[1,2] Danielle Stewart,[1,2] Zsuzsanna Fabry,[1,2] and Matyas Sandor[1,2,3]

[1]Department of Pathology and Laboratory Medicine, School of Medicine and Public Health, [2]Cellular and Molecular Pathology Training Program, and [3]Microbiology Doctoral Training Program, University of Wisconsin, Madison, Wisconsin, USA.

An estimated one-third of the world's population is infected with *Mycobacterium tuberculosis*, although most affected individuals maintain a latent infection. This control is attributed to the formation of granulomas, cell masses largely comprising infected macrophages with T cells aggregated around them. Inflammatory DCs, characterized as $CD11c^+CD11b^+Ly6C^+$, are also found in granulomas and are an essential component of the acute immune response to mycobacteria. However, their function during chronic infection is less well understood. Here, we report that $CD11c^+$ cells dynamically traffic in and out of both acute and chronic granulomas induced by *Mycobacterium bovis* strain bacillus Calmette-Guérin (BCG) in mice. By transplanting *Mycobacterium*-induced granulomas containing fluorescently labeled $CD11c^+$ cells and bacteria into unlabeled mice, we were able to follow $CD11c^+$ cell trafficking and T cell activation. We found that half of the $CD11c^+$ cells in chronic granulomas were exchanged within 1 week. Compared with tissue-resident DC populations, $CD11c^+$ cells migrating out of granuloma-containing tissue had an unexpected systemic dissemination pattern. Despite low antigen availability, systemic $CD4^+$ T cell priming still occurred during chronic infection. These data demonstrate that surveillance of granulomatous tissue by $CD11c^+$ cells is continuous and that these cells are distinct from tissue-resident DC populations and support T cell priming during both stages of *Mycobacterium* infection. This intense DC surveillance may also be a feature of *Mycobacterium tuberculosis* infection and other granuloma-associated diseases.

Introduction

The initiation and maintenance of an adequate cellular immune response have enabled an estimated 2 billion people worldwide to control, but rarely eliminate, infection with *Mycobacterium tuberculosis* (1). This control requires the formation of granulomas, the histopathologic hallmark of disease comprising infected macrophages surrounded by a close aggregation of leukocytes. The close interaction of antigen-specific T cells and infected macrophages afforded by the granuloma architecture enables the host to contain infection and prevent dissemination (2). The role DCs play during early mycobacteria infection has recently been characterized and is now considered an essential cellular component in the initiation of adaptive immunity (3). By transiently depleting DCs using pCD11c-diphtheria toxin receptor transgenic mice or by eliminating a primary chemokine network utilized by DCs en route to lymph nodes using *plt* mice, which lack CCR7 ligands CCL19 and CCL21ser, recent studies have demonstrated the necessity of mycobacteria transport and subsequent T cell activation by DCs (4, 5).

The presence of DCs in both human and murine *M. tuberculosis* and bacillus Calmette-Guérin (BCG) chronic granulomas is appreciated; however, their exact role during this time is unknown (6–9). When addressing the role of DCs during chronic infection, it is critical to take into account that acute and chronic granulomas are different in terms of their cellular composition, bacterial load, and cytokine and chemokine milieu (10). It is unknown whether these differences allow for antigenic sampling, DC trafficking, and a sustained *Mycobacterium*-specific T cell response during chronic infection.

In the present study, we investigate DC migration into and out of both acute and chronic BCG–induced granulomas. While the BCG infection model in mice has its limitations compared with that of *M. tuberculosis* infection, it also has its advantages. *M. tuberculosis* burden in mice remains stable throughout infection, with mice eventually succumbing to disease (11, 12). However, the strong majority of humans infected with *M. tuberculosis* control infection for an often long, indefinite period of time. Unlike *M. tuberculosis*, mice infected with BCG also control infection. Currently, there are limited models to address granuloma traffic and antigenic sampling in the mammalian system. A study by Egen et al. elegantly demonstrated the continuous movement of T cells and relative immobility of macrophages within the granuloma (13). Again, using intravital 2-photon microscopy, this same group more recently demonstrated that myeloid and lymphoid populations in *M. tuberculosis*–induced hepatic granulomas behaved the same as in BCG-induced granulomas in terms of motility and T cell arrest (14). A study by Davis et al. tracked macrophage egression from primary granulomas during early infection of *Mycobacterium marinum* in zebra fish embryos (15). However, neither of these studies investigated DC motility. Here, we present a kidney capsule liver transplant model that allows us to monitor DC migration into and egression from both acute and chronic granulomas and the resulting T cell response. Collectively, these data demonstrate that $CD11c^+$ cells enter and exit, although at different rates, both acute and chronic *Mycobacterium*–induced granulomas. Interestingly, compared with naive tissue, we observed

Conflict of interest: The authors have declared that no conflict of interest exists.
Citation for this article: *J Clin Invest.* 2011;121(10):3902–3913. doi:10.1172/JCI45113.

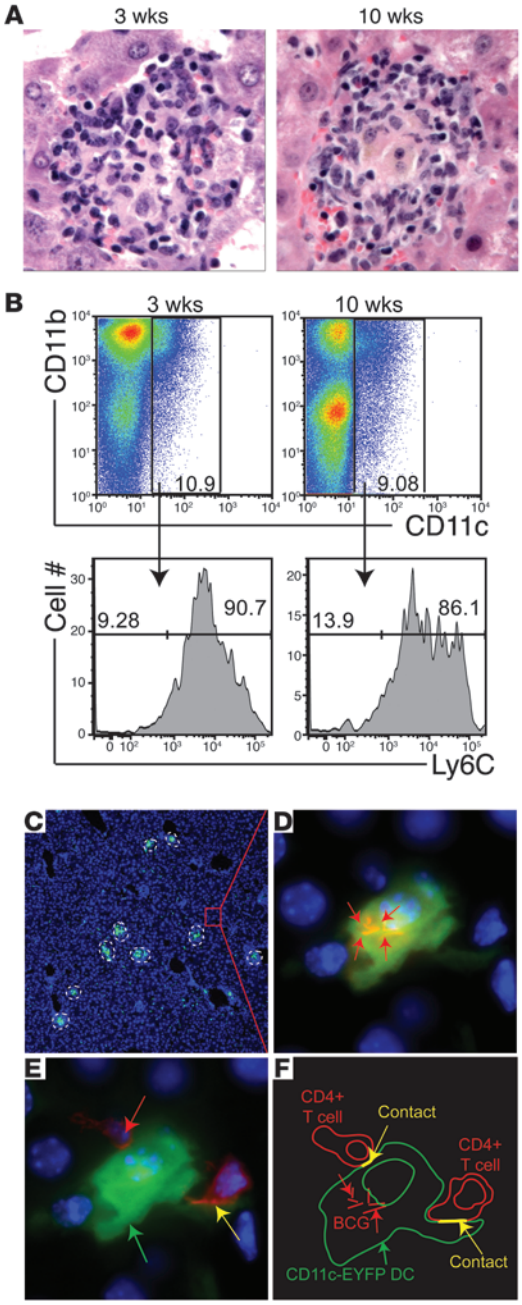

Figure 1
CD11c⁺ cells in acute and chronic granulomas. C57BL/6 mice were systemically infected i.p. with BCG. (**A**) H&E staining of formalin-fixed liver tissue showing 3- and 10-week granulomas. Original magnification, ×400. (**B**) Top panels, CD11c and CD11b populations in liver granuloma cell suspensions. Plot obtained by gating on the population displaying high side scatter (SSC) and forward scatter (FSC), excluding lymphocytes. Numbers within gate denote frequency of CD11c⁺ cells within high SSC and high FSC population. Bottom panels, Ly6C expression on gated CD11c⁺ population from above plots. Gate set based on known Ly6C-negative populations and numbers denote distribution of Ly6C-positive and -negative expression on CD11c⁺ population. (**C**) Original magnification, ×100. Fluorescent microscopy image taken of liver from CD11c-EYFP mouse infected for 10 weeks with dsRED BCG. Granulomas outlined with white dashed lines. CD11c-EYFP cells are shown in green, and DAPI nuclear stain in blue. (**D**) Digital magnification of red box in **C**. Original magnification, ×1000. Red arrows point to dsRED BCG rods. (**E**) CD11c-EFYP cell from **D** with anti-CD4 staining (red). Red arrow points to CD4⁺ cell, and yellow arrow points to merged CD4⁺YFP⁺ staining. Original magnification, ×1000. (**F**) Representation of observations in **D** and **E**. Representative plots and images from at least 3 or more independent experiments.

that CD11c⁺ cells leaving both 3- and 10-week-infected tissue had a unique systemic dissemination pattern. We found that the early, continuous CD11c⁺ surveillance and CCR7-dependent migration to the lymph node supported T cell activation, but the recipients' MHCII⁺ cells were necessary to prime *Mycobacterium*-specific T cells during both phases of infection.

Results

Both acute and chronic BCG-induced granulomas contain a population of CD11c⁺ cells, which can be found harboring mycobacteria outside granulomas in chronically infected mice. Acute granulomas (3 weeks after infection) are generally more numerous and less well organized compared with chronic granulomas (10 weeks after infection) (Figure 1A and Figure 2, B and C). It is well known that the acute lesions have both a high bacterial burden and a high frequency of IFNγ⁺CD4⁺ T cells, while the latter chronic granulomas have less of both (10). Acute granulomas are associated with a high incidence of bacterial killing, while chronic lesions are associated with long-term bacterial survival (16). The 10-week chronic granuloma typically has 2–3 logs fewer bacilli than 3-week acute lesions. One point of view is that this difference in bacterial burden may be the single most important factor responsible for the changing immunological microenvironment within the granuloma. Figure 1B shows that both acute and chronic granulomas contain similar proportions of CD11c⁺CD11b⁺Ly6C⁺ cells (Figure 1B). This subset is often referred to as the monocyte-derived "inflammatory" DC subset (17, 18). Support for a population of DCs capable of migrating into and out of chronic granulomas came from observing liver sections of 10-week dsRED BCG-infected CD11c enhanced yellow fluorescent protein (CD11c-EYFP) mice with ubiquitously fluorescing DCs (19). Albeit rare, CD11c-YFP⁺ cells containing dsRED bacilli could be observed outside of granulomas in chronically infected mice (Figure 1, C–F). Costaining with anti-CD4 often revealed these cells in close contact with CD4⁺ T cells (Figure 1, E and F). Unbeknownst to the origin or destination of this observed BCG-infected CD11c⁺ cell, this finding also demonstrates the limitations of the current model for studying DC traffic into and out of granulomas and the subsequent need for a new methodical approach.

Liver tissue containing intact granulomas with mycobacteria and CD11c-EYFP⁺ cells can be transplanted underneath the kidney capsule of a recipient. In order to better study the traffic of CD11c⁺ cells from granulomatous lesions, we have made use of the well-characterized kidney capsule transplant protocol to develop a model to track, quantify, and measure CD11c⁺ cellular traffic, along with the immunological outcome (20). The kidney capsule transplantation is a well-characterized model that has been used for decades based on the fact that it is one of the highly vascularized regions in the body. Complete revascularization of the graft only takes several days, resulting in a highly oxygenized graft. With a skilled hand, close to 100% of the grafts are accepted and the wound heals properly. This model is achieved by systemically

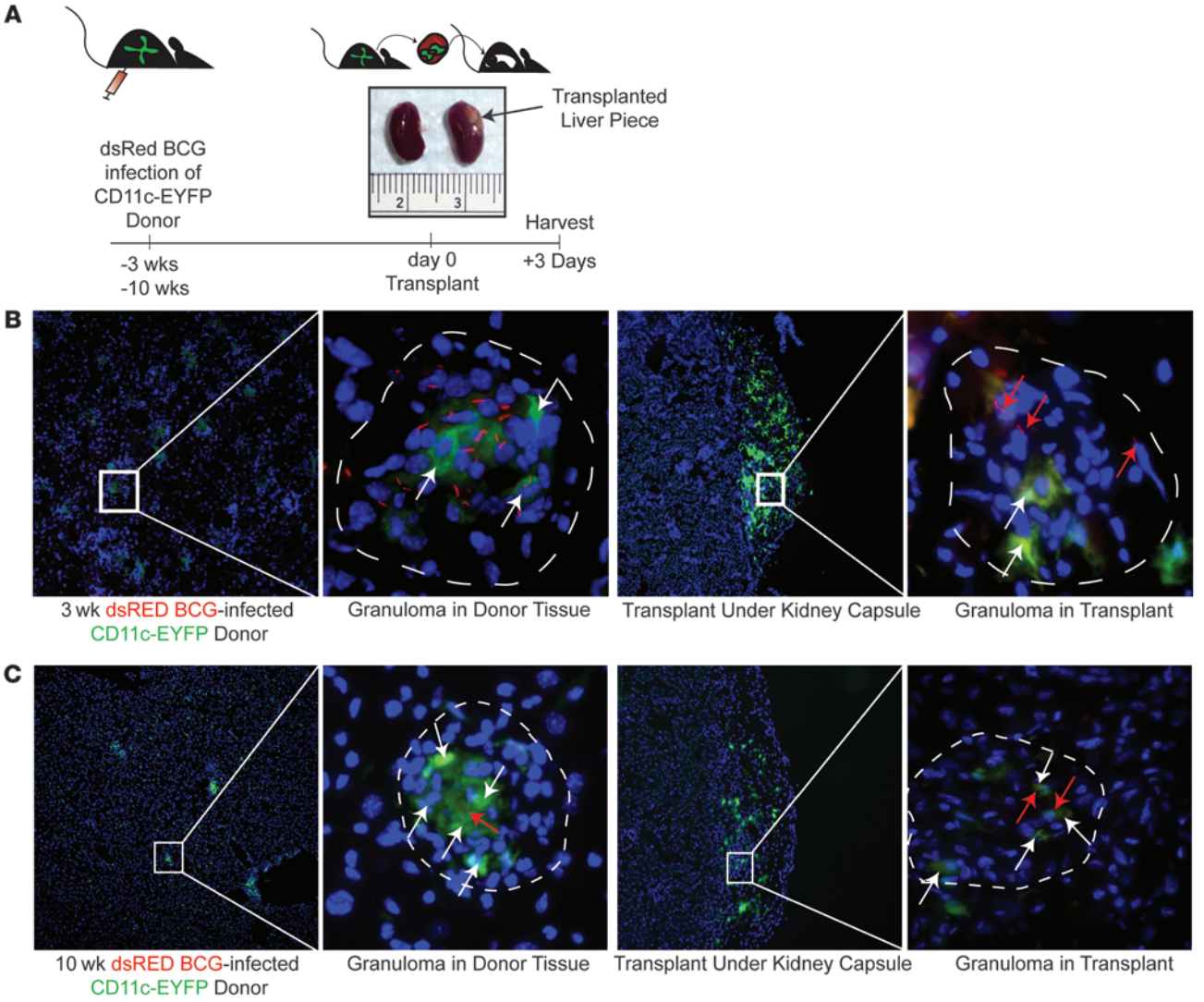

Figure 2

Transplantation of liver granulomas under recipient's kidney capsule. (**A**) Schematic of transplantation model. Liver specimen (~0.025 g ± 10%) containing granulomas from a 3- or 10-week dsRED BCG–infected CD11c-EYFP donor mouse is transplanted underneath the kidney capsule of a colorless C57BL/6 recipient. (**B** and **C**) CD11c-EYFP mice infected 3 weeks (**B**) and 10 weeks (**C**). Far left images show infected liver; original magnification, ×400. Second column shows white-boxed granuloma; original magnification, ×1000. White arrows point to CD11c-EYFP$^+$ cells within granuloma, and red arrows point to dsRED BCG. Third column shows CD11c-EYFP liver specimen under kidney capsule of colorless recipient; original magnification, ×100. Far right column demonstrates transplanted granulomas containing both CD11c-EYFP$^+$ cells (white arrows) and dsRED BCG (red arrows); original magnification, ×1000. 3- and 10-week-infected donor images representative of 3 independent experiments each, and transplanted kidney capsule images are representative of 3–6 mice per time point from 3 or more independent experiments.

infecting CD11c-EYFP mice with dsRED BCG and waiting until either acute or chronic lesions are formed within the liver (Figure 2, B and C). As depicted in Figure 2A, a small piece (0.025 g ± 10%) of liver from the acutely or chronically infected CD11c-EYFP mouse is transplanted underneath the kidney capsule of a syngeneic WT recipient (Figure 2A). The images in Figure 2, B and C, show the transplanted YFP$^+$ liver piece underneath the capsule of a colorless recipient. Importantly, CD11c-EYFP$^+$ cells and dsRED BCG bacilli can be found in granulomatous lesions in the piece of transplanted liver (Figure 2, B and C). These data demonstrate both the feasibility of the transplant and ability to transfer either intact acute or chronic granulomatous lesions.

CD11c-EYFP$^+$ cells migrate out of both acute and chronic lesions to peripheral secondary organs. By transplanting granuloma-containing liver pieces from CD11c-EYFP$^+$ donors (Figure 3A), we can track YFP$^+$ cellular egression from granulomas. Sentinel CD11c-EYFP$^+$ cells are present in the noninfected liver (Figure 3A); however, many more CD11c-EYFP$^+$ cells are present in infected livers (Figure 3A). At both acute and chronic infection time points, there are fewer CD11c-EYFP$^+$ cells in the interstitial tissue space outside granulomas compared with an uninfected liver (Figure 3A). When quantified, in both acute and chronic stages, the statistical majority of CD11c-EYFP$^+$ cells are associated with granulomatous lesions ($P = 0.0001$ and $P = 0.0004$, respectively) (Figure 4A). This may be

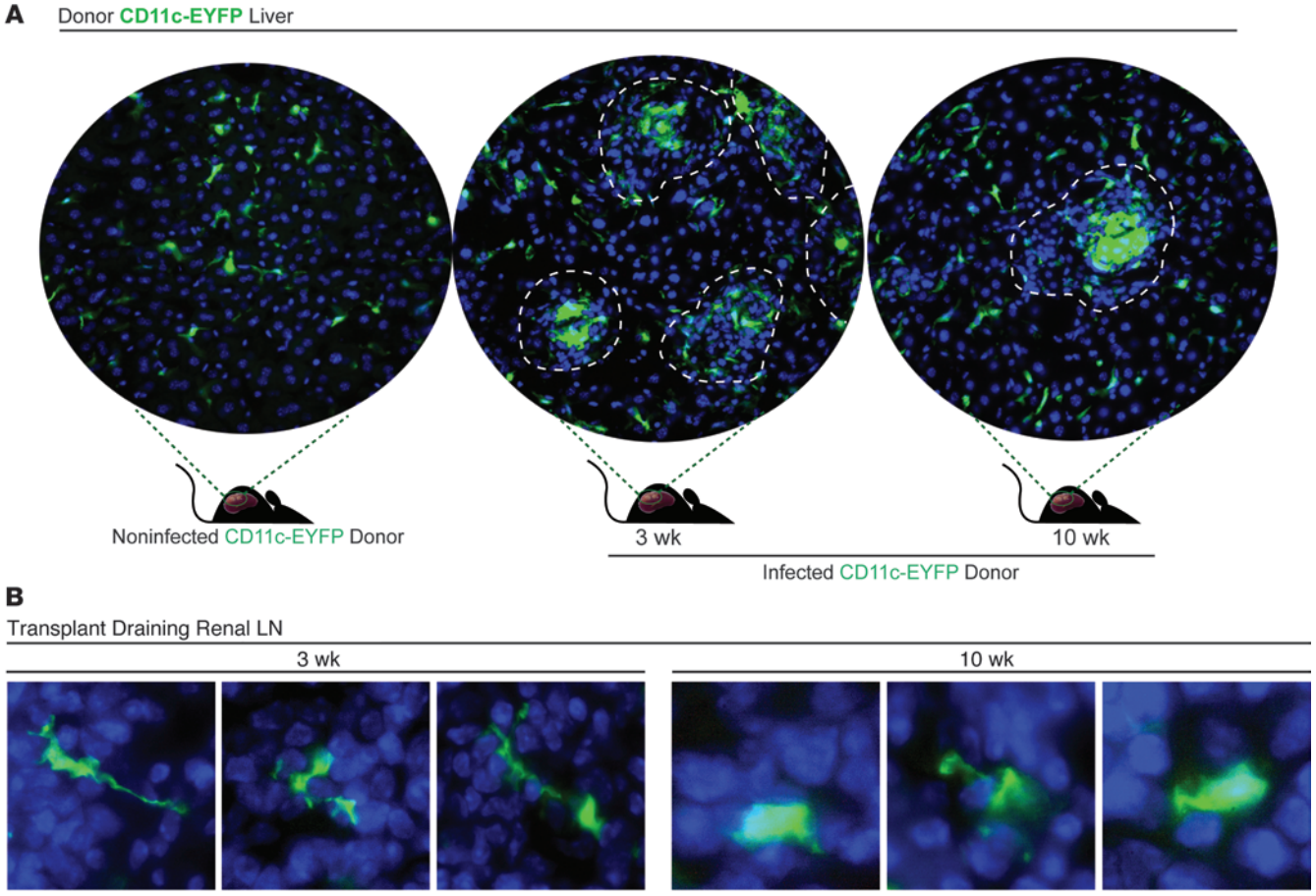

Figure 3
Migration of CD11c-EYFP cells out of transplant. (**A**) CD11c-EYFP distribution in donor liver tissue of noninfected (left), 3-week-infected (middle), and 10-week-infected (right). Original magnification, ×400. (**B**) In both recipients of acute and chronic infected donors, CD11c-EYFP cells were found in the tRLN 3 days after transplant. Original magnification, ×1000 magnification. Images representative from at least 3 or more independent experiments.

due to the migration of stressed liver-resident DCs to the draining lymph nodes or into the granulomas. The latter is less likely, as most of the CD11c$^+$ cells in the granulomas are Ly6C$^+$, strongly suggestive of their hematogenous arrival (21). Nevertheless, it is important to note that the vast majority of transplanted CD11c-EYFP$^+$ cells are granuloma associated. Fluorescent microscopy of the sectioned tRLN 3 days after transplant revealed the presence of YFP$^+$ cells (Figure 3B). Although rare, both the inherent fluorescence and morphological dendrite protrusions make these cells easily distinguishable as transplant-originated DCs. Validating our previous observation from Figure 1, which suggests a CD11c$^+$ population capable of migrating out of chronic lesions, we were able to find YFP$^+$ DCs in the tRLN of both 3- and 10-week-infected mice (Figure 3B). Interestingly, we have never found a dsRED BCG rod in any of the CD11c-EYFP$^+$ cells that have migrated from the transplant. This observation was further strengthened by CFU on lymph nodes, spleen, and liver, which were repeatedly negative (Supplemental Figure 1; supplemental material available online with this article; doi:10.1172/JCI45113DS1). To confirm that viable BCG remained in the transplanted granulomas over the course of infection, we removed the grafted liver piece 14 days following transplant and performed CFU and a thorough microscopy search for fluorescent BCG (Supplemental Figure 1A). Indeed, viable BCG was still present and contained within the grafted liver piece throughout the duration of our experiments. To further confirm the viability of BCG within the graft, we removed the transplanted liver piece and grafted into TNF-α–deficient recipients. TNF-α is required to maintain the granulomas' cellular composition and anti-bacterial dissemination properties (22). Under TNF-α–deficient conditions, the BCG was not contained and disseminated. In accordance, transplantation of Rag-deficient donors into WT also does not contain infection and dissemination is observed (Supplemental Figure 1B). We concluded that over the course of our investigational period, the BCG localization and viability remain constant. Having immunocompetent donors and recipients is sufficient to contain the infection within the granuloma and at the same time maintain *Mycobacterium* viability.

CD11c-EYFP$^+$ cells migrating out of both acute and chronic infected donor tissue have a systemic dissemination pattern, but differ in the quantity and rate of egression. To systemically track CD11c-EYFP$^+$ cell egression from the transplanted granulomas, we used real-time PCR to measure YFP transcript (Figure 4, B and C). A standard curve was generated from known quantities of purified CD11c-EYFP$^+$ cells diluted into WT YFP$^-$ cells (Figure 4B). The equation generated from the

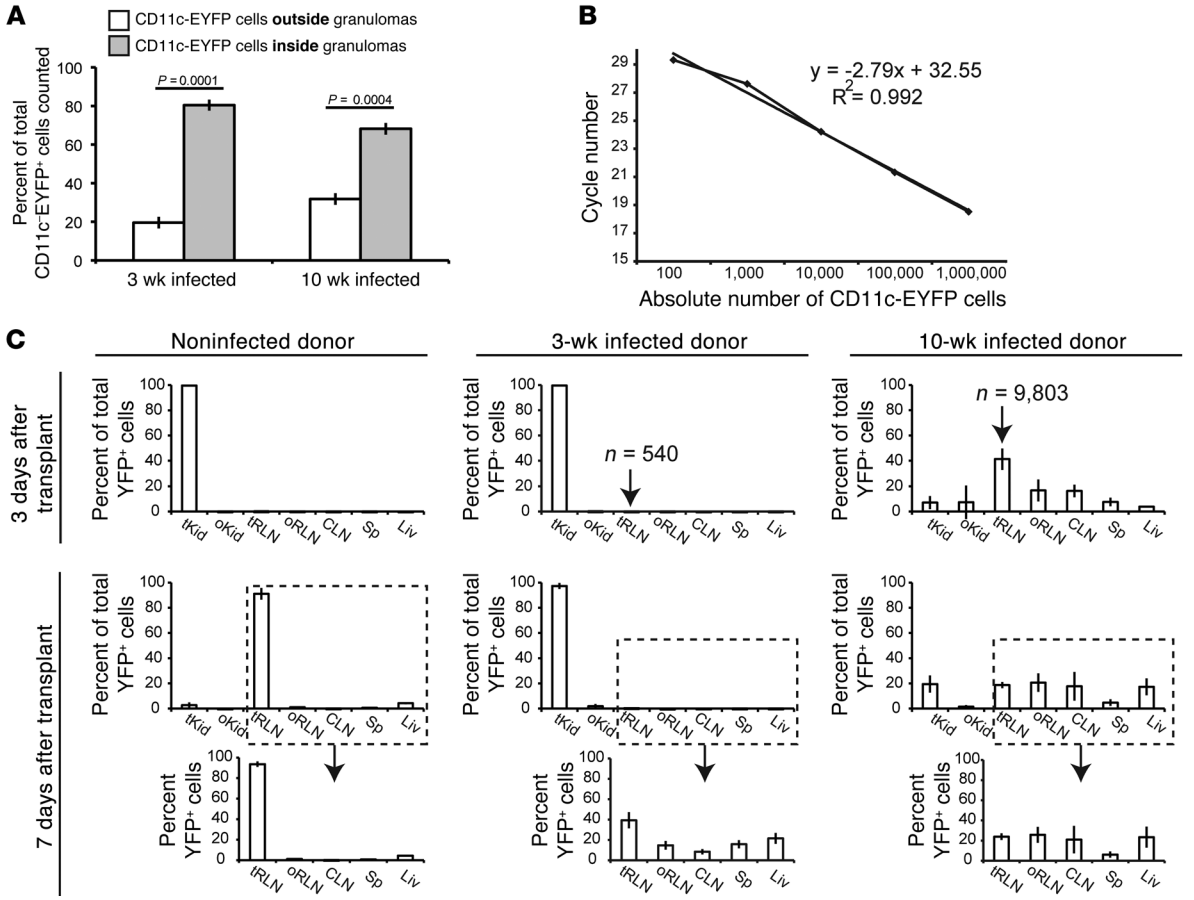

Figure 4
CD11c-EYFP cells migrate out of transplanted granuloma-containing liver piece to systemic sites. (**A**) Distribution of CD11c-EYFP cells in donor liver. All CD11c-EYFP cells in 10–15 ×400 objective fields from 3 mice per time point were counted and determined to be either within or outside of granulomas, determined by DAPI nuclear stain. (**B**) Real-time PCR standard curve generated from known values of purified CD11c-EYFP cells diluted into WT cells. (**C**) 3 (top row) and 7 (bottom 2 rows) days after transplant, RT-PCR was performed to detect YFP transcript from transplanted kidney (tKid), opposite kidney (oKid), transplant-draining renal lymph node (tRLN), opposite renal lymph node (oRNL), cervical lymph nodes (CLN), spleen (Sp), and liver (Liv). Graphs show percentage of total YFP⁺ cells detected by PCR. Bottom row shows total percentage distribution of disseminated YFP⁺ cells from dashed box above, and *n* value above box indicates absolute total number of YFP⁺ cells. Error bars represent mean ± SEM and data representative of 3 independent experiments per time point with 2–3 mice per group.

standard curve along with whole and partial organ weights were used henceforth to determine the absolute number of CD11c-EYFP⁺ in various tissues. At 3 and 7 days after transplant of liver pieces from noninfected or 3- or 10-week BCG infected CD11c-EYFP mice, the transplanted kidney, opposite kidney, transplant-draining renal lymph node (tRLN), opposite renal lymph node, cervical lymph nodes, spleen, and liver were removed and homogenized (Figure 4C). Real-time PCR was performed on total isolated RNA from tissue homogenate to detect YFP transcript. At 3 days after transplant, the vast majority of CD11c-EYFP⁺ cells remained in both the noninfected and 3-week-infected donor liver; however, 41% ± 13% migrated out of the chronic 10-week-infected donor piece to all peripheral sites sampled, particularly the tRLN. On average, the 10-week tRLN contained 9,803 CD11c-EYFP⁺ cells compared with 540 and 46 in the 3-week and noninfected tRLNs, respectively. At 7 days after transplant, those CD11c-EYFP⁺ cells that regressed from the acute transplant also migrated to all sampled systemic organs, but those from the noninfected liver migrated nearly exclusively to the tRLN. Interestingly, these data demonstrate that compared with noninfected tissue, CD11c⁺ cells originating from acutely or chronically *Mycobacterium*-infected tissue have the ability to disseminate to peripheral sites. Furthermore, for what we believe is the first time, these data also suggest that DCs presumably associated with chronic granulomas readily migrate to secondary lymphoid organs, and compared with DCs from noninfected tissue, DCs from *Mycobacterium*-infected tissue have a different migratory route given their different end points.

Recipient CD11c⁺ cells migrate into chronic transplanted granulomas more than into acute granulomas. After observing different patterns of DC egression from acute and chronic lesions, we next determined whether the same was true for recipient CD11c⁺ cells' access into transplanted granulomas by transplanting uninfected or 3- or 10-week-infected colorless C57BL/6 liver pieces under the kidney capsule of CD11c-EYFP mice. At 3 and 7 days after transplant, the transplanted liver piece was excised, homogenized, and analyzed by flow cytometry (Figure 5A). To determine the distribution of

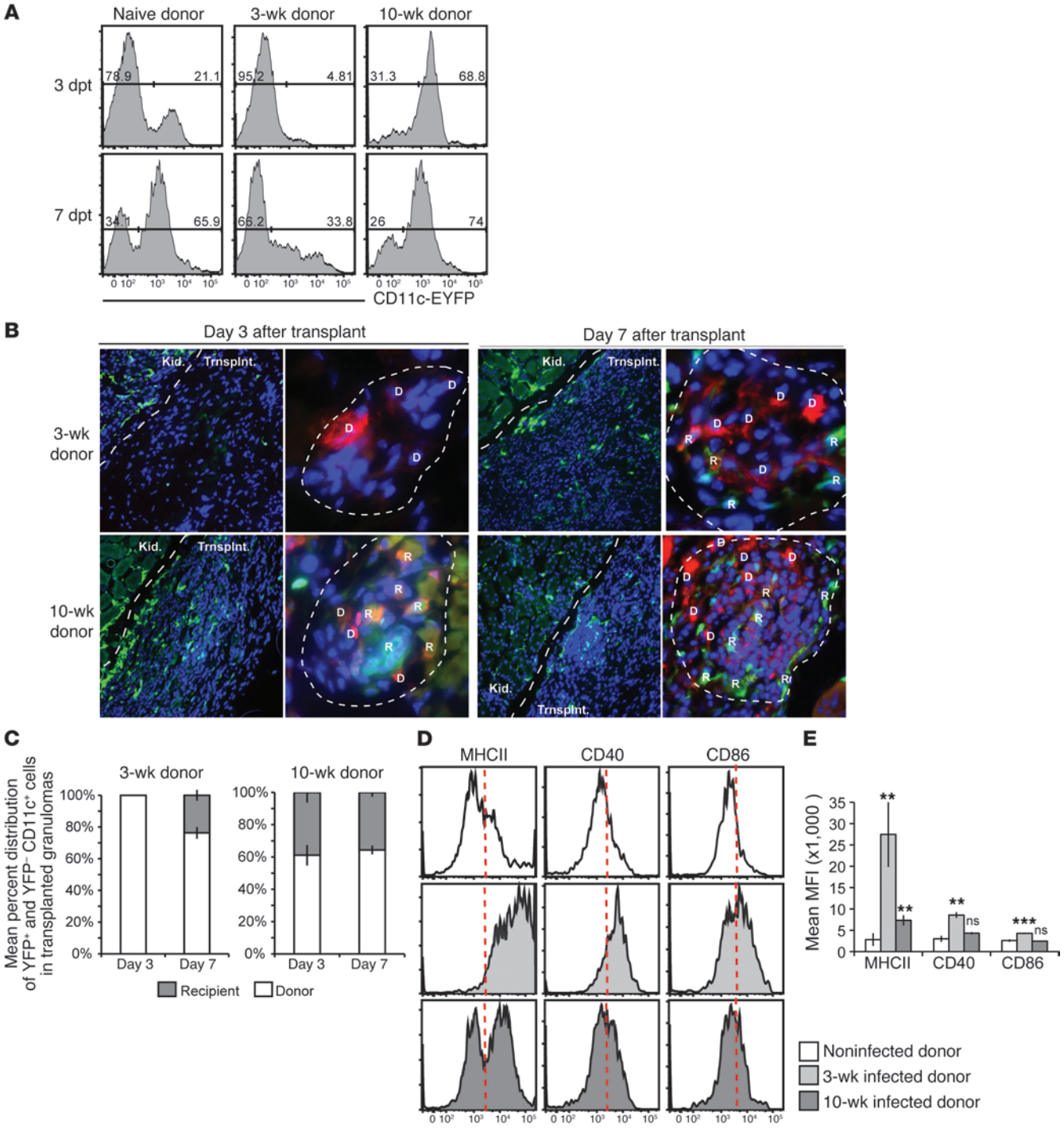

Figure 5

CD11c-EYFP+ migration into transplanted granulomas. Noninfected or 3- or 10-week-infected liver pieces from colorless donors were transplanted into CD11c-EYFP recipients. (**A**) 3 and 7 days post transplant (dpt), donor liver tissue was excised and prepared for flow cytometry. CD11c-EYFP histograms generated from CD11c+ surface stain gate. Numbers denote frequency of CD11c-EYFP positive and negative cells among total CD11c+ population. (**B**) Fluorescent microscopy images of transplanted kidney 3 and 7 days after transplant. In first and third columns, white dashed lines indicate borders of transplanted piece and kidney. In second and fourth columns, red indicates donor anti-CD11c surface stain (D), and green or yellow/orange indicate recipient CD11c+ cell (R). Original magnification, ×400 (first and third columns); ×1000 (second and fourth columns). D, donor; R, recipient. (**C**) Mean distribution of all donor (white bars) and recipient (gray bars) CD11c+ cells per granuloma 3 and 7 days after transplant. CD11c+ cellular distribution was determined from 10 granulomas per time point. (**D**) Histograms showing surface expression of MHCII and activating costimulatory molecules CD40 and CD86. Red dashed line represents background expression. (**E**) Mean MFI of MHCII and costimulatory molecule expression. Data shown representative of 2 independent experiments with 4 kidneys per group. $^{**}P < 0.05$; $^{***}P < 0.001$. Error bars represent mean ± SEM.

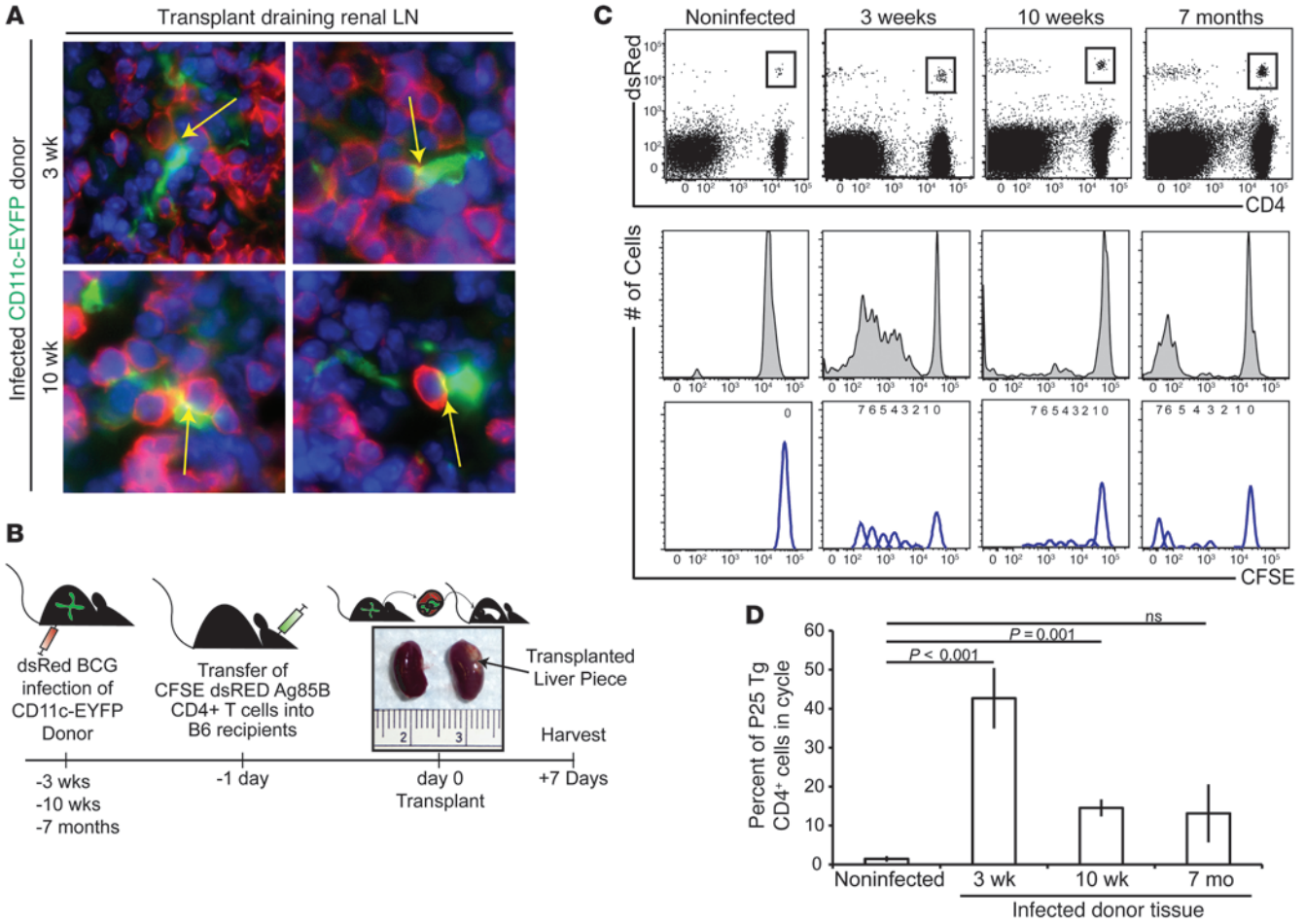

Figure 6

Proliferation of Mycobacteria-specific Ag85B CD4+ T cells after transplant of acutely and chronically infected liver tissue. (**A**) Fluorescent microscopy of transplant tRLN 7 days after transplant. CD11c-EYFP cells (green), and CD4+ T cells (red). Yellow arrows point to merged green and red staining. Original magnification, ×1000. (**B**) Experimental schematic. Briefly, CD11c-EYFP mice were systemically infected with dsRED BCG for 3 weeks, 10 weeks, or 7 months. 1 day prior to transplant, 5×10^5 CFSE-labeled dsRED Ag85B CD4+ T cells were adoptively transferred. 7 days after transplant, the tRLNs were removed and analyzed by flow cytometry. (**C**) Top row: adoptively transferred Tg T cells were identified by CD4+dsRED+ gating, plots shown were obtained from lymphocyte gate on SSC versus FSC plot. Bottom 2 rows: CFSE dilution histogram from Tg gate from upper row. (**D**) Graph shows average percentage of dsRED Ag85B CD4+ T cells in cycle. Graph representative of 2–5 independent experiments per time point with an average of 2–6 mice per group. Error bars represent mean ± SEM, and statistical significance between groups is shown in graph.

donor CD11c+ cells and recipient CD11c+ cells in the transplant, histograms were generated from the surface-stained CD11c+ gate and evaluated for YFP+ fluorescent expression. Interestingly, CD11c-EYFP+ cells readily migrated into noninfected and 10-week chronically infected donor tissue by day 3, where a minority (~5%) of CD11c+ cells in the acute donor were of recipient origin (Figure 5A). By 7 days after transplant, approximately 75% of CD11c+ cells in the chronically infected donor tissue were newly recruited recipient CD11c+ cells. This suggests a high turnover of granuloma-associated CD11c+ cells in these lesions. The visible network of sentinel kidney YFP+CD11c+ cells afforded us the ability to easily detect the colorless transplanted piece by fluorescent microscopy (Figure 5B). At 3 days after transplant, recipient CD11c-EYFP+ cells (R) had already infiltrated chronic granulomas and could be found in both the periphery and center of the lesions (Figure 5B), whereas few recipient CD11c-EYFP+ cells could be found in acute 3-week granulomas. Only donor CD11c+ cells (D) could be found in acute lesions (Figure 5B). Unlike the chronic donor, by day 7 after transplant, those CD11c-EYFP+ cells that had infiltrated the acute donor tissue were found primarily in the lymphocytic cuff around the lesions (Figure 5B). Like the distribution of EYFP- and EYFP+CD11c+ cells observed within the entire transplant by flow cytometry (Figure 5A), a similar pattern was observed locally within the granuloma after quantifying the distribution of donor CD11c+ cells and recipient CD11c-EYFP+ cells on a single lesion basis (Figure 5C). Together with the previous observation that CD11c+ cells egress from chronic granulomas faster than from acute lesions, these data collectively demonstrate that after transplantation, chronic granulomas are more quickly infiltrated by recipient CD11c+ cells compared with acute granulomas.

Once recipient CD11c+ cells migrate into the transplanted granulomas, their maturation status is likely to respond accordingly. Previously, we found that CD11c+ cells in acute granulomas were extremely activated with high expression of MHCII and T cell

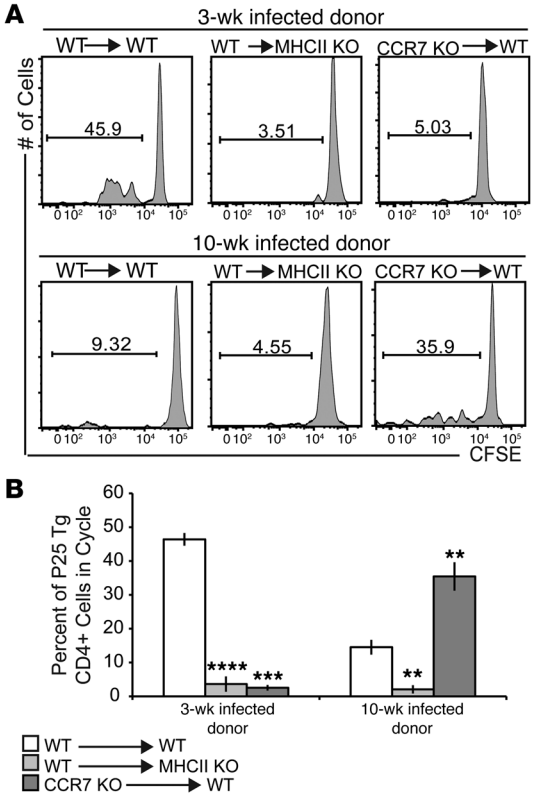

Figure 7

Mycobacteria-specific Ag85B CD4+ T cell proliferation is dependent on MHCII expression on recipients' cells. (**A**) 5 × 10^5 CFSE-labeled dsRED P25 CD4+ T cells were adoptively transferred into recipient C57BL/6 mice or MHCII-deficient mice 1 day prior to transplant of 3- and 10-week BCG-infected WT donors (3–5 mice per time point representative of 1–3 independent experiments), and 3- and 10-week BCG-infected *Ccr7*$^{-/-}$ donors (6 mice per time point). CFSE dilution histogram of Tg P25 CD4+ T cells in the tRLN 7 days after transplant. Numbers denote frequency of proliferating cells determined by set gate. Cells shown from same Tg gating strategy used in Figure 6C. (**B**) Mean percentage of P25 Tg CD4+ T cells 7 days after transplant in tRLN in cycle. Values obtained from gating strategy shown in **A**. Statistical significance from WT is as follows: ****P = 0.00001; ***P = 0.0001; **P = 0.001. Error bars represent mean ± SEM.

costimulatory molecules CD40 and CD86 (21). However, CD11c+ cells in chronic lesions of both BCG-infected mice and the lungs of *M. tuberculosis*–infected mice had much lower expression of these markers (21, 23). Here, we found that when the CD11c-EYFP+ cells migrated into either uninfected or 3- and 10-week-infected transplants, they achieved a maturation status similar to that of the resident CD11c+ cells. Compared with CD11c-EYFP+ cells that entered either noninfected or 10-week chronically infected tissue, those found in 3-week-infected donor tissue had significantly higher expression of MHCII and T cell costimulatory molecules CD40 and CD86 (Figure 5, D and E), thus demonstrating, that newly arrived CD11c+ cells in the granuloma take on the phenotype of the resident CD11c+ cells.

Antigenic sampling results in proliferation of mycobacteria-specific Ag85B CD4+ T cells after transplant of acutely and chronically infected BCG and M. tuberculosis liver granulomas. One of the questions that remain regarding infection with pathogenic mycobacteria is whether there is continuous antigenic sampling from chronic granulomas and subsequent T cell priming. However, in order to ask this question, one has to rule out the presence of mycobacteria in the lymph nodes where priming occurs and rule out the possibility of T cell priming as a result of newly formed lesions during chronic time points. The transplant model presented here allows us to address the question of antigenic sampling from chronic lesions. We have observed migration of CD11c-EYFP+ cells in and out of both acute and chronic granuloma–laden transplants (Figures 3–5). Collectively, our data demonstrate that a portion of CD11c+ cells within the chronic granuloma are able to reach the draining lymph nodes, the primary site of T cell priming. To see whether newly emigrated CD11c-EYFP+ cells engage with T cells in the tRLN, we used fluorescent microscopy (Figure 6A). CD11c-EYFP+ cells from both 3- and 10-week-infected donors were found in close contact with CD4+ T cells (Figure 6A). To test whether T cell priming occurred, donor CD11c-EYFP mice were infected for 3 weeks, 10 weeks, or 7 months (Figure 6B). Uninfected CD11c-EYFP mice were used as negative controls. One day prior to transplant, all mice received an adoptive transfer of 5 × 10^5 CFSE-labeled dsRED P25 CD4+ T cells, which have TCR specificity for *Mycobacterium* Ag85B of *M. tuberculosis* and BCG. On the day of the transplant, C57BL/6 recipients received a piece of either uninfected or 3-week, 10-week, or 7-month infected liver. Seven days after transplant, P25 CD4+ T cells in the transplanted tRLN were analyzed by flow cytometry (Figure 6C). P25 CD4+ T cells were traced by co-CD4 and -dsRED expression. CFSE dilution of these cells was observed in all infected donor recipients (Figure 6C). Compared with the noninfected antigen-free donor, statistically more P25 CD4+ T cells were in cycle in both the acute and chronic infected donor groups and detectable in the 7-month donor recipient as well (Figure 6D). In addition to BCG, we examined P25 CD4+ T cell priming after transplant of both 3- and 10-week *M. tuberculosis* strain mc²6020 (Δ*lysA* Δ*panCD* mutant), auxotrophic for lysine and pantothenate, infected liver (Supplemental Figure 2). Infection with this *M. tuberculosis* mutant results in 2 features similar to latency: low CFU and a nonproliferative state (24). We found that T cell priming occurred after transplant of both acute and chronic *M. tuberculosis*-induced granulomas. However, due to the low bacterial load observed with this strain, both time points resulted in similar levels of T cell priming. These data begin to address the long-standing question of continuous T cell priming during chronic *Mycobacterium* infection. Although not as robust as in response to acute lesions, which have a much higher bacterial burden, here we show that systemic *Mycobacterium*-specific CD4+ T cells divide after transplant of both 10-week and 7-month chronic donors, despite the low bacterial burden.

Recipient MHCII molecule expression is required for priming of P25 CD4+ T cells following transplant of both acutely and chronically infected liver granulomas. As previously mentioned, the DCs associated with *Mycobacterium*-induced granulomas are of the myeloid monocyte–derived "inflammatory" DC subset, characterized by CD11c^{int-hi}CD11b^{hi}Ly6C^{hi}. However, previous studies investigating the P25 CD4+ T cell activation capacity of this subset during early *M. tuberculosis* infection found them to be poor T cell stimulators that elicit much less IFN-γ production compared with other DC subsets (5). There is a paradigm that newly arrived migratory DCs in the lymph node tend to "hand off" antigen to lymph node–

resident DCs (25, 26). To determine whether the granuloma-originated DCs were responsible for T cell activation or whether the recipients' DCs were acquiring antigen and priming, we adoptively transferred 5×10^5 CFSE-labeled dsRED P25 CD4$^+$ T cells into MHCII-deficient recipients and transplanted 3- or 10-week-infected liver pieces from MHCII-expressing donors. Seven days after transplant, P25 CD4$^+$ T cells in the transplanted kidney-draining renal lymph node were analyzed by flow cytometry (Figure 7A). In both 3- and 10-week-infected donor MHCII-deficient recipients, the frequency of P25 CD4$^+$ T cells in cycle was significantly decreased (Figure 7, A and B). These data indicate that granuloma MHCII$^+$ cells are not sufficient for priming *Mycobacterium*-specific P25 CD4$^+$ T cells. This would suggest that recipient MHCII$^+$ cells obtain antigen. The acquisition of antigen by recipient DCs may occur within the lymph node after the migration of granuloma-derived APCs, or within the transplant by obtaining antigen from resident macrophages or DCs, or engulfing any extracellular bacteria. In recipients of both 3- and 10-week-infected donors, we found CD11c-EYFP$^+$ recipient cells in close proximity with donor CD11c$^+$ cells within the transplant (Supplemental Figure 3A) and recipient CD11c-EYFP$^+$ cells with viable dsRED BCG at 7 days after transplant of a 3-week-infected donor (Supplemental Figure 3B). Furthermore, 3- and 10-week donor CD11c-EYFP$^+$ cells could be found in direct contact with recipient CD11c$^+$ cells in the draining renal lymph nodes (Supplemental Figure 3C). Based on the previous observation that CD11c$^+$ cells are able to readily infiltrate chronic, but not acute, granulomas by day 3, we hypothesized that if antigenic transfer required the shuttling of mycobacterial antigen to the lymph nodes by granuloma CD11c$^+$ cells, this could be facilitated by either donor or recipient CD11c$^+$ cells during chronic infection, but only donor CD11c$^+$ cells during acute infection. To test this, we transplanted liver pieces from 3- and 10-week-infected CCR7-deficient mice. CCR7, chemokine receptor 7, is expressed by DCs and T lymphocytes and is a receptor responsible for DC migration to the lymph nodes in response to ligands CCL19 and CCL21 (27). The *Ccr7*$^{-/-}$ mice had a similar proportion and localization of CD11c$^+$ cells in the granuloma at both 3- and 10-week infection time points (data not shown). Transplant of 3-week-infected *Ccr7*$^{-/-}$ mice resulted in a significant decrease in P25 activation (Figure 7, A and B). However, after transplantation of 10-week-infected *Ccr7*$^{-/-}$ donor liver, the level of P25 CD4$^+$ T cell activation surpassed that observed in 10-week WT donors (Figure 7, A and B). The bacterial burden in a 10-week *Ccr7*$^{-/-}$ animal is slightly higher as compared with 10-week WT (data not shown), which could result in higher antigen availability and, therefore, increased priming.

Discussion

DC function is inherently associated with migration from the site of immune surveillance to the draining lymph node. The use of DC, T cell, and bacteria-specific fluorescent coding, in combination with the well-characterized kidney capsule transplant model presented here, allows us to ask questions regarding DC migration to and from granulomas and the potential consequence(s) it may have on the immune response. This model addresses granuloma-antigen priming by excluding the possibility of extra-granulomatous bacteria or the possibility of T cell priming as a result of newly formed lesions. Additionally, the transplantation itself also bears medical relevance, as tuberculosis remains a serious risk to liver transplant recipients Although most instances are the result of reactivation of latent *M. tuberculosis* in the recipient following transplantation, there are cases of transmission through the transplanted liver, particularly in developing countries (28, 29). Along with its advantages, the transplant model also has several restrictions. Like any surgery, the physical stress of the transplant itself is likely to induce nonspecific migration; however, the environment surrounding the granulomatous inflammation may be similarly stressed. We include noninfected transplants to establish a baseline as an important control. Importantly, tissue integrity of the transplant for the duration of these studies (≤ 7 days) is excellent and granulomas within the transplant can be easily detected.

On a cellular level, our data support a changing view of chronic granulomas by showing that one-third of DCs are exchanged by traffic in and out of the granuloma within 1 week. Interestingly, we found that CD11c$^+$ cells had significantly better access to enter and exit chronic granulomas compared with acute. This finding was unexpected, considering the robust inflammation associated with acute lesions. One would expect considerable CD11c$^+$ recruitment during this time due to a stronger chemokine gradient (30). Additionally, the extracellular matrix that surrounds both acute, and to a somewhat higher extent, chronic granulomas, does not seem to prevent the entry of CD11c$^+$ cells into chronic lesions. Additional studies are needed to understand why chronic granulomas, the predominate site of long-term bacterial persistence, are so thoroughly exposed to immune-surveying cells.

We were also able to track the migration of CD11c$^+$ cells out of acute and chronic granulomas. Interestingly, compared with CD11c-EYFP$^+$ cells associated with uninfected tissue, which solely migrated to the transplant-draining renal lymph node, CD11c-EYFP$^+$ cells originating from granulomas disseminated to many systemic sites (Figure 4). This may be attributed to the subset of DCs associated with uninfected and infected tissue. The former subset includes interstitial liver DCs, predominantly comprising CD11c$^+$CD11b$^+$Ly6c$^-$ DCs (31), whereas the DC subset almost exclusively associated with *Mycobacterium* inflammation in the acute and chronic granuloma are the monocyte-derived inflammatory (CD11b$^+$CD11c$^+$Ly6C$^+$) DCs (21). The stress of the surgery associated with the transplant may be sufficient to induce the migration of tissue-resident DCs in the uninfected transplant to drain into the renal lymph node. However, the activated CD11b$^+$CD11c$^+$Ly6C$^+$ DCs in the infected tissue are more equipped to migrate to many systemic sites following transplantation. It will be important to determine whether inflammatory DCs in other infectious models have the same systemic migration pattern or whether this is unique to the mycobacterial granuloma system. DC migration is indispensable for immune surveillance, making future studies investigating the underlying mechanism for this migration pattern necessary in order to better understand chronic *Mycobacterium* infection.

We demonstrate here that there is antigenic sampling from the chronic granulomas, therefore supporting the hypothesis that despite low antigenic levels in chronic lesions, localized bacteria sustain a systemic immune response. By 7 days after transplant of acute and chronic BCG- and *M. tuberculosis* mc^{2}6020–induced granulomas, adoptively transferred *Mycobacteterium*-specific P25 CD4$^+$ T cells proliferated (Figure 6 and Supplemental Figure 2). Future studies will require investigation of chronic pulmonary granulomas induced by virulent *M. tuberculosis* and during human disease. The presence of mycobacterial antigen–containing DCs in the lymph nodes of *M. tuberculosis*–infected individuals already sug-

gests a level of continuous antigenic priming; however, the source and arrival time of that antigen is unknown (8). Antigenic priming during chronic stages was further supported by a recent study that identified latent antigen-specific T cells in the peripheral blood of latently infected individuals (32).

To better understand the relative role of donor granuloma APCs and recipient APCs in acute and chronic priming of granuloma antigen, we used both chemokine receptor– and MHCII-deficient mice (Figure 7). The lack of P25 $CD4^+$ T cell priming observed when WT tissue was transplanted into MHCII-deficient recipients demonstrates an absolute requirement for recipient APCs. This was not surprising, as the same subset of DCs involved with *M. tuberculosis* infection have been shown to be poor inducers of Th1 immunity (5). Accordingly, a recent study by McCurley and Mellman found that this monocyte-derived subset in humans quickly degrades intracellular antigen, which is likely to affect antigen presentation and T cell priming (33). We observed both donor $CD11c^+$–recipient $CD11c^+$ contact locally within the transplant and within the draining lymph node, an accepted site for DC-DC antigen exchange. We also noticed recipient $CD11c^+$ cells with BCG in the transplant (Supplemental Figure 3). While these data only provide indirect evidence for DC-DC antigen exchange, they do support the feasibility of recipient $MHCII^+$ cells obtaining antigen for priming. T cell priming did not occur after transplant of a CCR7 KO acute 3-week donor, suggesting that DC traffic to the draining lymph nodes is required for T cell priming. However, transplant of a CCR7 KO chronic 10-week donor resulted in T cell priming. Considering the higher traffic of DCs into chronic granulomas, it is likely that CCR7-sufficient recipient DCs are recruited into the lesion, obtain antigen, and carry it to the lymph node. A recent study by Celli and colleagues demonstrating the early infiltration of inflammatory monocytes and DCs into allografted ear tissue and their ability to ferry antigen to the draining lymph node for T cell activation is in accordance with our observations (34). Collectively, these data suggest that priming in response to acute infection requires that antigen be shuttled to the lymph node by granuloma-originating $CCR7^+$ APCs and this process is abrogated in either MHCII-deficient recipients or CCR7-deficient donors. Even with sufficient antigen pick-up by incoming $CD11c^+$ cells, priming during chronic stage was also entirely dependent on MHCII expression on recipient APCs.

Data presented in this study demonstrate that $CD11c^+$ cells have access to both acute and chronic granulomas, but once inside, they acquire a different phenotype. $CD11c^+$ cells in acute granulomas express molecules that support T cell reactivation, while $CD11c^+$ cells in chronic lesions display a more tolerogenic phenotype (Figure 5, D and E). Recently, we reported that the change in $CD11c^+$ phenotype may affect IFN-γ availability within the granuloma and alter the bactericidal capacity of the granulomatous environment (21). A more recent intravital imaging study by Egen and colleagues demonstrated that newly recruited, primed P25 $CD4^+$ T cells did not form long-lasting engagements with granuloma APCs due to insufficient antigen presentation (14). Not only does this support our finding that granuloma $CD11c^+$ cells are poor inducers of T cell priming, but it further highlights the fact that cellular recruitment and interactions within the granuloma microenvironment dramatically influence the immune response and disease course.

Imaging *Mycobacterium*-induced granulomas has significantly increased our understanding of mycobacterial pathophysiology (13, 35, 36). Here, we present a new approach for studying $CD11c^+$ cellular traffic and T cell priming from granulomas that combines both cell- and bacteria-specific fluorescence and transplantation. The chronic granuloma is thought to be the site where low levels of bacteria can survive indefinitely. A better understanding of specific immunity during the late phase of infection will help us better understand and treat latent mycobacterial infections. As a blood-derived cell, the inflammatory DC subset may also play an important role in other infectious granuloma models. In addition to *Mycobacterium*-induced granulomas, cells making up leishmania- and schistosome-induced granulomas and autoimmune-associated granulomas (i.e., Crohn and sarcoidosis) are also largely recruited from the blood. Future studies investigating the traffic of this DC subset to and from these lesions and the effect they have on local and systemic immunity, will also be significant.

Methods

Mice. C57BL/6 ($H2^b$), CCR7-deficient (B6.129P2(C)-*Ccr7*^{tm1Rfor}/J), and Actb-DsRED.T3 Tg mice were purchased from Jackson Laboratory. CD11c-EYFP Tg mice on the C57BL/6 background were a gift from Michel C. Nussenzweig (Rockefeller University, New York, New York, USA) (19). P25 transgenic mice were a gift from Antonio G. Rothfuchs and Alan Sher (NIH, Bethesda, Maryland, USA). MHCII-deficient mice were a gift from Chella David (Mayo Clinic, Rochester, Minnesota, USA). P25 mice were bred with Actb-DsRED.T3 transgenic mice to obtain dsRED P25 mice. Mice were housed and bred in a pathogen-free facility at the University of Wisconsin Animal Care Unit (Madison, Wisconsin, USA) according to the guidelines of the Institutional Animal Care and Use Committee.

Infection. Kanamycin-resistant dsRED-expressing BCG, a gift from Lalita Ramakrishnan (University of Washington, Seattle, Washington, USA), was grown in Middlebrook 7H9 supplemented with 0.05% Tween 80 and 10% oleic acid–dextrose–catalase supplement (Difco) in the presence of kanamycin (50 μg/ml) and stored at –80°C. *M. tuberculosis* strain mc^26020 (Δ*lysA* Δ*panCD* mutant) was a gift from William R. Jacobs Jr. (Albert Einstein College of Medicine, New York, New York, USA) and grown as previously described (24). For infections, ampoules were thawed, diluted in PBS, and briefly sonicated to obtain single-cell suspensions. For systemic infection, a nonlethal dose of 1×10^7 CFU in 100 μl was i.p. injected. CFU on liver, spleen, and lymph node homogenates was performed as previously described (37).

Transplant. Mice were anesthetized by i.p. injection of a ketamine (90 mg/kg)/xylazine (10 mg/kg) mixture and s.c. injected with meloxicam for pain management. An area on the dorsal side of the mouse toward the posterior end was shaved and swabbed with iodine. A 1-cm longitudinal incision through the skin and peritoneum was made above the last rib and hip joint, and the kidney then withdrawn. A 1-mm incision along the kidney capsule was made and the capsule then drawn away from the kidney, creating an open pocket between the organ and the capsule. Two pieces of donor liver of approximately 0.025 g ± 10% in mass were inserted under the capsule. The peritoneum was then sutured and the skin incision closed with surgical staples. Mice received kanamycin (5 mg/kg) in their water 1 day prior to surgery and for the duration of their recovery.

Mononuclear cell isolation and flow cytometry. Isolation of splenocytes, lymph nodes, and granuloma-infiltrating cells was performed as previously described (38). Transplanted liver tissue was processed between 2 glass slides and treated with 5 mg/ml type I collagenase (Sigma-Aldrich) at 37°C for 40 minutes with shaking. The softened granulomas were disrupted by repeated expulsion through a syringe for 1 minute and washed. Isolated cells were processed for flow cytometry. A total of 10^6 cells was incubated

for 30 minutes on ice with saturating concentrations of labeled Abs with 40 μg/ml unlabeled 2.4G2 mAb to block binding to Fc receptors and washed 3 times with staining buffer (PBS plus 1% BSA). Fluorochrome-labeled Abs against CD11c (HL3), CD11b (Mac-1), MHCII I-A^b (AF6-120.1), CD40 (3/23), and CD86 (GL1) were purchased from BD Biosciences. Anti-CD16/CD32 (2.4G2) was produced from hybridomas. Cell surface staining was acquired on a FACSCalibur or LSRII (BD Biosciences) and analyzed with FlowJo (Tree Star) software, version 5.4.5.

Fluorescent microscopy. Organs fixed overnight in 3% formalin/25% sucrose in PBS were frozen in O.C.T. Compound (Tissue-Tek Sakura). 5- to 10-μm–thick cryosections were cut from O.C.T.-embedded tissue samples and fixed for 10 minutes in ice-cold acetone, then washed 3 times with PBS and outlined with a Pap pen. Sections were then surface stained, with 40 μg/ml of 2.4G2 blocking Ab, for 2 hours at room temperature in PBS and washed with PBS for 30 minutes. Sections were mounted using ProLong Gold Antifade Reagent with DAPI (Invitrogen). All images were acquired with a camera (Optronics Inc.) mounted on a fluorescence microscope (Olympus BX41; Leeds Precision Instruments). PictureFrame software (Optronics Inc.) was used to obtain JPEG images.

Real-time PCR. For standard curve, $CD11c^+$ cells were purified from CD11c-EYFP transgenic mice using a CD11c MicroBeads Cell Separation Kit from Miltenyi Biotec. Greater than 90% purity was confirmed by flow cytometry. Known quantities of purified CD11c-EYFP cells were diluted into WT cells and lysed in TRIzol Reagent (Invitrogen). Total RNA was extracted and reverse transcribed using MMLV reverse transcriptase (Invitrogen) using oligo(dT) as primer according to the manufacturer's protocol. Real-time PCRs were performed using the following YFP primers: forward 5′-CCACATGAAGCAGCAGGACTT-3′ and reverse 5′-GGTGCGCTCCTGGACGTA-3′ (Integrated DNA Technologies), β2-microglobulin primers (sense) 5′-TGACCGGCTTGTATGCTATC-3′ and (antisense) 5′-CAGTGTGAGCCAGGATATAG-3′, and 10,000-fold diluted SYBR Green stock solution (Molecular Probes) in a Smart Cycler version 1.2f (Cepheid). For real-time PCR on tissue samples, both whole organs and fractions of organs were weighed prior to homogenization. To both determine standard curve and quantify absolute number of YFP^+ cells, PCR curves were plotted on a logarithmic scale to reveal exponential growth region. Cycle number at the log fluorescence of 10 was determined and plotted against original YFP^+ dilution. Threshold values of log fluorescence 10 were determined for the various tissues, and corresponding cycle number was plugged into equation generated from the standard curve.

Adoptive transfer. Pooled splenocytes and lymphocytes from dsRED P25 transgenic mice were CFSE labeled as previously described (39) (Molecular Probes). 5×10^5 $V\beta11^+CD4^+$ transgenic cells were adoptively transferred i.v. via retroorbital injection into recipient mice 1 day prior to transplant.

Statistics. Results are given as means ± SEM or means ± SD. Comparisons between groups was done using Student's 2-tailed *t* test analysis. $P < 0.05$ was considered significant.

Study approval. All animal experiments were approved by the Animal Care and Use Committee of the University of Wisconsin.

Acknowledgments

We would like to thank Toshi Kinoshita for expert histopathology services and members of our laboratory for helpful discussions and constructive criticisms of this work. We express special thanks to Michel C. Nussenzweig (Rockefeller University, New York, New York, USA), Antonio G. Rothfuchs and Alan Sher (NIH, Bethesda, Maryland, USA), and Chella David (Mayo Clinic, Rochester, Minnesota) for their gift of the CD11c-EYFP, P25, and MHCII KO mice, respectively. Also, thank you to William Jacobs (Albert Einstein College of Medicine) for his gift of *M. tuberculosis* strain mc^26020, and Lalita Ramakrishnan (University of Washington) for her gift of the dsRED BCG plasmid. Work was supported by the Bill and Melinda Gates Foundation, and NIH funding R01-A1048087 and R21-A1072638 (to M. Sandor).

Received for publication September 14, 2010, and accepted in revised form July 20, 2011.

Address correspondence to: Matyas Sandor, 5468 MSC, 1300 University Ave., Madison, Wisconsin 53705, USA. Phone: 608.265.8715; Fax: 608.262.0846; E-mail: msandor@wisc.edu.

Heidi A. Schreiber's present address is: The Rockefeller University, New York, New York, USA.

1. Ulrichs T, Kaufmann SH. New insights into the function of granulomas in human tuberculosis. *J Pathol*. 2006;208(2):261–269.
2. Saunders BM, Britton WJ. Life and death in the granuloma: immunopathology of tuberculosis. *Immunol Cell Biol*. 2007;85(2):103–111.
3. Cooper AM. Cell-mediated immune responses in tuberculosis. *Annu Rev Immunol*. 2009;27:393–422.
4. Tian T, Woodworth J, Skold M, Behar SM. In vivo depletion of CD11c+ cells delays the CD4+ T cell response to Mycobacterium tuberculosis and exacerbates the outcome of infection. *J Immunol*. 2005;175(5):3268–3272.
5. Wolf AJ, et al. Mycobacterium tuberculosis infects dendritic cells with high frequency and impairs their function in vivo. *J Immunol*. 2007;179(4):2509–2519.
6. Schreiber HA, Sandor M. The role of dendritic cells in mycobacterium-induced granulomas. *Immunol Lett*. 2010;130(1–2):26–31.
7. Uehira K, et al. Dendritic cells are decreased in blood and accumulated in granuloma in tuberculosis. *Clin Immunol*. 2002;105(3):296–303.
8. Tailleux L, et al. DC-SIGN is the major Mycobacterium tuberculosis receptor on human dendritic cells. *J Exp Med*. 2003;197(1):121–127.
9. Tsai MC, et al. Characterization of the tuberculous granuloma in murine and human lungs: cellular composition and relative tissue oxygen tension. *Cell Microbiol*. 2006;8(2):218–232.
10. Co DO, Hogan LH, Kim SI, Sandor M. Mycobacterial granulomas: keys to a long-lasting host-pathogen relationship. *Clin Immunol*. 2004;113(2):130–136.
11. Hingley-Wilson SM, Sambandamurthy VK, Jacobs WR Jr. Survival perspectives from the world's most successful pathogen, Mycobacterium tuberculosis. *Nat Immunol*. 2003;4(10):949–955.
12. Flynn JL. Lessons from experimental Mycobacterium tuberculosis infections. *Microbes Infect*. 2006;8(4):1179–1188.
13. Egen JG, Rothfuchs AG, Feng CG, Winter N, Sher A, Germain RN. Macrophage and T cell dynamics during the development and disintegration of mycobacterial granulomas. *Immunity*. 2008;28(2):271–284.
14. Egen JG, Rothfuchs AG, Feng CG, Horwitz MA, Sher A, Germain RN. Intravital imaging reveals limited antigen presentation and T cell effector function in mycobacterial granulomas. *Immunity*. 2011;34(5):807–819.
15. Davis JM, Ramakrishnan L. The role of the granuloma in expansion and dissemination of early tuberculous infection. *Cell*. 2009;136(1):37–49.
16. Thompson-Snipes L, Skamene E, Radzioch D. Acquired resistance but not innate resistance to Mycobacterium bovis bacillus Calmette-Guerin is compromised by interleukin-12 ablation. *Infect Immun*. 1998;66(11):5268–5274.
17. Leon B, Lopez-Bravo M, Ardavin C. Monocyte-derived dendritic cells. *Semin Immunol*. 2005;17(4):313–318.
18. Geissmann F, Manz MG, Jung S, Sieweke MH, Merad M, Ley K. Development of monocytes, macrophages, and dendritic cells. *Science*. 2010; 327(5966):656–661.
19. Lindquist RL, et al. Visualizing dendritic cell networks in vivo. *Nat Immunol*. 2004;5(12):1243–1250.
20. Robertson NJ, Fairchild PJ, Waldmann H. Ectopic transplantation of tissues under the kidney capsule. *Methods Mol Biol*. 2007;380:347–353.
21. Schreiber HA, et al. Dendritic cells in chronic mycobacterial granulomas restrict local anti-bacterial T cell response in a murine model. *PLoS One*. 2010;5(7):e11453.
22. Kindler V, Sappino AP, Grau GE, Piguet PF, Vassalli P. The inducing role of tumor necrosis factor in the development of bactericidal granulomas during BCG infection. *Cell*. 1989;56(5):731–740.
23. Gonzalez-Juarrero M, Orme IM. Characterization of murine lung dendritic cells infected with Mycobacterium tuberculosis. *Infect Immun*. 2001;69(2):1127–1133.
24. Sambandamurthy VK, et al. Long-term protection against tuberculosis following vaccination with a severely attenuated double lysine and pantothenate auxotroph of Mycobacterium tuberculosis. *Infect Immun*. 2005;73(2):1196–1203.
25. Belz GT, et al. Distinct migrating and nonmi-

grating dendritic cell populations are involved in MHC class I-restricted antigen presentation after lung infection with virus. *Proc Natl Acad Sci U S A*. 2004;101(23):8670–8675.
26. Allan RS, et al. Migratory dendritic cells transfer antigen to a lymph node-resident dendritic cell population for efficient CTL priming. *Immunity*. 2006;25(1):153–162.
27. Lukacs-Kornek V, Engel D, Tacke F, Kurts C. The role of chemokines and their receptors in dendritic cell biology. *Front Biosci*. 2008;13:2238–2252.
28. Singh N, Paterson DL. Mycobacterium tuberculosis infection in solid-organ transplant recipients: impact and implications for management. *Clin Infect Dis*. 1998;27(5):1266–1277.
29. Yehia BR, Blumberg EA. Mycobacterium tuberculosis infection in liver transplantation. *Liver Transpl*. 2010;16(10):1129–1135.
30. Peters W, Ernst JD. Mechanisms of cell recruitment in the immune response to Mycobacterium tuberculosis. *Microbes Infect*. 2003;5(2):151–158.
31. Sumpter TL, Abe M, Tokita D, Thomson AW. Dendritic cells, the liver, and transplantation. *Hepatology*. 2007;46(6):2021–2031.
32. Schuck SD, et al. Identification of T-cell antigens specific for latent mycobacterium tuberculosis infection. *PLoS One*. 2009;4(5):e5590.
33. McCurley N, Mellman I. Monocyte-derived dendritic cells exhibit increased levels of lysosomal proteolysis as compared with other human dendritic cell populations. *PLoS One*. 2010;5(8):e11949.
34. Celli S, Albert ML, Bousso P. Visualizing the innate and adaptive immune responses underlying allograft rejection by two-photon microscopy. *Nat Med*. 2011;17(6):744–749.
35. Volkman HE, Pozos TC, Zheng J, Davis JM, Rawls JF, Ramakrishnan L. Tuberculous granuloma induction via interaction of a bacterial secreted protein with host epithelium. *Science*. 2010;327(5964):466–469.
36. Ulrichs T, et al. Modified immunohistological staining allows detection of Ziehl-Neelsen-negative Mycobacterium tuberculosis organisms and their precise localization in human tissue. *J Pathol*. 2005;205(5):633–640.
37. Co DO, et al. Interactions between T cells responding to concurrent mycobacterial and influenza infections. *J Immunol*. 2006;177(12):8456–8465.
38. Hogan LH, et al. Mycobacterium bovis strain bacillus Calmette-Guerin-induced liver granulomas contain a diverse TCR repertoire, but a monoclonal T cell population is sufficient for protective granuloma formation. *J Immunol*. 2001;166(10):6367–6375.
39. Ling C, Sandor M, Suresh M, Fabry Z. Traumatic injury and the presence of antigen differentially contribute to T-cell recruitment in the CNS. *J Neurosci*. 2006;26(3):731–741.